ARTICLES

Electrochemistry, Spectroscopy, and Electrogenerated Chemiluminescence of Some Star-Shaped Truxene−Oligofluorene Compounds†

Khalid M. Omer,‡ Alexander L. Kanibolotsky,§,£ Peter J. Skabara,§ Igor F. Perepichka,£,#,¶ and Allen J. Bard*,‡

Center of Electrochemistry, Chemistry and Biochemistry Department, The University of Texas at Austin, Austin, Texas 78712, WestCHEM, Department of Pure and Applied Chemistry, University of Strathclyde, Glasgow G1 1XL, U.K., L. M. Litvinenko Institute of Physical Organic and Coal Chemistry, National Academy of Sciences of Ukraine, Donetsk 83114, Ukraine, and Department of Chemistry, Durham University, Durham DH1 3LE, U.K.

Received: January 29, 2007; In Final Form: March 12, 2007

We report electrochemical studies, spectroscopy, and electrogenerated chemiluminescence (ECL) of four monodisperse star-shaped truxene core−oligofluorene compounds (**T1**−**T4**). All oligomers produced stable radical anions and radical cations and showed blue ECL by ion annihilation with an intensity that could be seen with the naked eye. ECL spectra showed that all ECL emissions were at the same position as the fluorescence emission, except for **T1**, the compound with the shortest fluorene arms that produced some longer wavelength emission in addition to that seen in the fluorescence spectrum. When tetra-*n*-butylammonium oxalate was used as a coreactant for **T1**, the emission was much weaker than that in ion annihilation with the same long-wavelength emission observed, making it unlikely that this emission can be ascribed to excimer formation. The ECL intensity of **T4** was about 80% of the common blue ECL emitter, 9,10-diphenylanthracene (DPA), under similar conditions.

Introduction

Electrogenerated chemiluminescence (ECL) is a unique type of electron transfer that generates excited states by the reaction of radical ions (or other highly oxidized or reduced species). It has been extensively investigated and has found several applications.[1] Fluorene-based materials are often highly fluorescent species and are promising candidates for various optoelectronic applications. Over the past decade, polyfluorenes have emerged as leading electroluminescent materials in polymeric light-emitting devices (PLED) for display technologies, demonstrating bright-blue emission coupled with high charge mobility, excellent thermal and electrochemical stability, and tunable properties through chemical modifications and copolymerizations.[2] Other electronic and photonic applications of fluorene-based homopolymers and copolymers include, for example, photovoltaics,[3,4] field-effect transistors (FET),[5] and solid-state lasers.[6] Homologous series of oligofluorenes, as monodisperse, well-defined π-conjugated systems,[7] have been fruitful in providing a correlation between electronic, optical, morphological properties, and chemical structure and molecular conformation, serving as models for polyfluorenes and providing deep insights into the photophysics of this promising class of conjugated polymers.[8,9] They were also successfully used as efficient emitters in organic light-emitting devices (OLED).[9,10] Generally, the environmental stability of monodisperse oligofluorenes (toward photooxidation or as materials in devices) is higher than those of polyfluorenes.[11] With the polymer analogues, faster degradation and the appearance of undesirable green emission during the PLED operation occurs due to the formation of fluorenone defects on the polymer chains; this chemical instability serves to decrease the device performance by quenching emission.[12]

The basic reactions in these OLEDs/PLEDs are the same as that in ECL in solution where light emission is produced by an energetic electron-transfer reaction (equivalent to electron−hole recombination) between electrochemically generated species at an electrode. Typically in ECL, radical ions of an organic compound (A) are generated sequentially at the surface of an electrode by cycling the potential within a short time interval and react (annihilate) during their interdiffusion. The annihilation by ECL between cation and anion radicals produces an excited state (A^*) if the energy provided by the electron-transfer reaction is sufficient to produce A^*. When A^* is the singlet state, eqs 1−4, this is called the S-route or an "energy sufficient system"

$$A - e^- \rightarrow A^{+\bullet} \quad (1)$$

$$A + e^- \rightarrow A^{-\bullet} \quad (2)$$

† Part of the special issue "Norman Sutin Festschrift".

* To whom correspondence should be addressed. E-mail: ajbard@mail.utexas.edu.
‡ The University of Texas at Austin.
§ University of Strathclyde.
£ National Academy of Sciences of Ukraine.
Durham University.
¶ Current address: Durham University.

10.1021/jp070765u CCC: $37.00
Published on Web 04/27/2007

$$A^{+\bullet} + A^{-\bullet} \rightarrow {}^1A^* + A \quad (3)$$

$${}^1A^* \rightarrow A + h\nu \quad (4)$$

If the energy provided by the ion radicals is not sufficient to populate the singlet state, the triplet state can be populated (eq 5), followed by triplet−triplet annihilation to generate the singlet state (eq 6). This is called the T-route or an "energy deficient system"

$$A^{+\bullet} + A^{-\bullet} \rightarrow {}^3A^* + A \quad (5)$$

$${}^3A^* + {}^3A^* \rightarrow {}^1A^* + A \quad (6)$$

Another possibility, referred to as the E-route, results from the production of an excimer in the annihilation reaction (eq 7)

$$A^{+\bullet} + A^{-\bullet} \rightarrow (A_2)^* \quad (7)$$

$$(A_2)^* \rightarrow 2A + h\nu \quad (8)$$

ECL can also be produced by oxidation alone by using a coreactant, a compound that can produce a strong reducing agent from a reaction that follows the electrochemical ET reaction. These reductants must be energetic enough to react with the cation radicals of the emitters to produce their excited states. Typical coreactants for oxidations are tri-*n*-propylamine (TPrA), which produces a strong reducing agent (TPrA$^{\cdot}$),[13,14] and oxalate ($C_2O_4^{2-}$), which produces a strong reductant, $CO_2^{-\bullet}$.[15−17] Alternatively a coreactant can be used in a reducing step by an analogous route. For example, peroxydisulfate ($S_2O_8^{2-}$)[18] and benzoyl peroxide (BPO)[19,20] produce strong oxidizing agents upon reduction.

Star-shaped conjugated oligomers as intrinsically two-dimensional conjugates (compared to more widely studied linear 1D conjugated systems) have been of great interest in recent years. The 2D character of such architectures allows further deep insight into the electronic processes in these compounds, including aspects of electronic interactions between the arms, and opens the door for new materials for optoelectronics.[21] Various star-shaped conjugated oligomers with different cores and arms (oligofluorenes,[22,23] oligothiophenes,[24] oligo(phenylenevinylenes),[25] oligo(phenyleneethynylenes),[26] etc.) have been synthesized, and their applications in OLEDs,[22b−e] photovoltaics,[24f,g] FETs,[24b,e,f] and nonlinear optics[25c,27] have been demonstrated.

SCHEME 1: Truxene−Oligofluorenes (T1−T4)

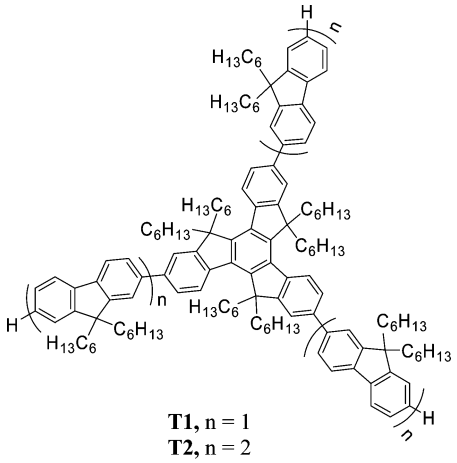

T1, n = 1
T2, n = 2
T3, n = 3
T4, n = 4

In this work, we describe the electrochemistry, spectroscopy, and ECL of a series of star-shaped oligofluorene compounds (Scheme 1). We describe both the electrochemistry and the spectroscopy of oligomers **T1**−**T4** containing an hexahexyl−truxene core with three oligofluorene arms of different lengths, from one fluorene unit (**T1**) to four fluorene units (**T4**) in the arms.

Experimental Section

Chemicals. The synthesis of **T1**−**T4** has been described previously.[23] Anhydrous acetonitrile (MeCN, 99.93% in a sure-

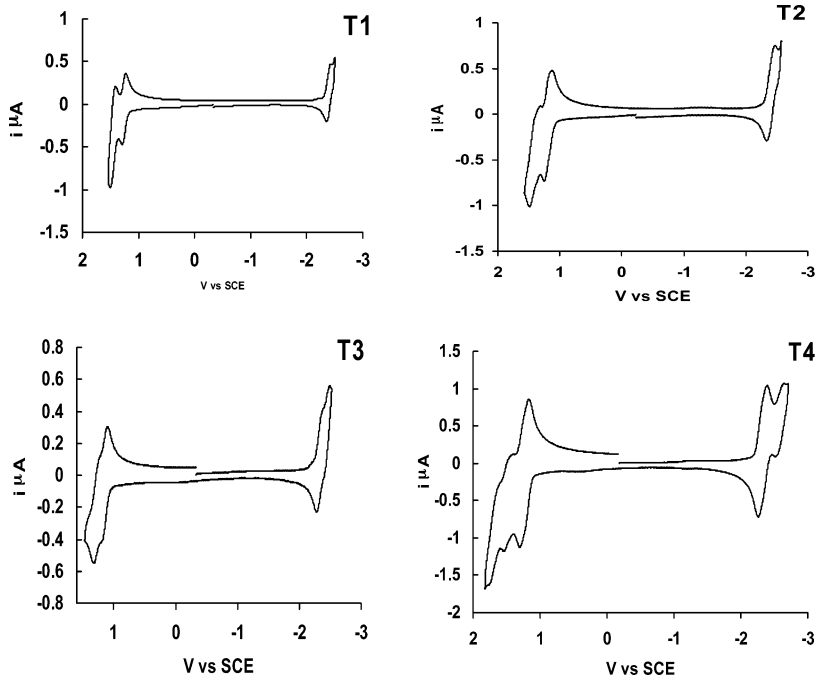

Figure 1. Cyclic voltammograms of **T1**−**T3** in MeCN/Bz (1:1 v/v) and **T4** in MeCN/Bz (1:2 v/v), 0.1 M $TBAPF_6$, with a scan rate of 0.5 V/s and a 0.5 mm Pt disc electrode.

TABLE 1: Summary of Electrochemical Data[a]

		oxidation peaks (V vs SCE)			reduction peaks (V vs SCE)			D cm^2/s
		first oxidation peak	second oxidation peak	third oxidation peak	first reduction peak	second reduction peak	third reduction peak	
T1	E_{pa}^{ox} or E_{pc}^{red} (exptl)	+1.28	+1.51		−2.52			
	E^o (from simulation)	+1.26	+1.47, +1.52		−2.45			7×10^{-6}
	n	1	2		1			
T2	E_{pa}^{ox} or E_{pc}^{red} (exptl)	+1.24	+1.48		−2.45			
	E^o (from simulation)	+1.20	+1.44, +1.49		−2.41			5×10^{-6}
	n	1	2		1			
T3	E_{pa}^{ox} or E_{pc}^{red} (exptl)	+1.24	+1.4		−2.30	−2.46		
	E^o (from simulation)	+1.20	+1.34		−2.27	−2.41		3×10^{-6}
	n	1	1		1	1		
T4	E_{pa}^{ox} or E_{pc}^{red} (exptl)	+1.23	+1.35	+1.54[b]	−2.23	−2.31	−2.57	
	E^o (from simulation)	+1.20	+1.29	+1.52	−2.20	−2.27	−2.52	1×10^{-6}
	n	1	1	1	1	1	1	

[a] All electrochemical measurements were performed at a ~0.5 mm Pt disc electrode in MeCN/Bz (1:1 v/v) for **T1**−**T3** and MeCN/Bz (1:2 v/v) for **T4**; E^o was obtained by simulation, E_{pa}^{ox} is the anodic peak potential for the oxidation process, E_{pc}^{red} is the cathodic peak potential for the reduction process, and n is number of electrons involved in the electron transfer. [b] There is another irreversible peak at +1.79, which is partially overlapped with the solvent.

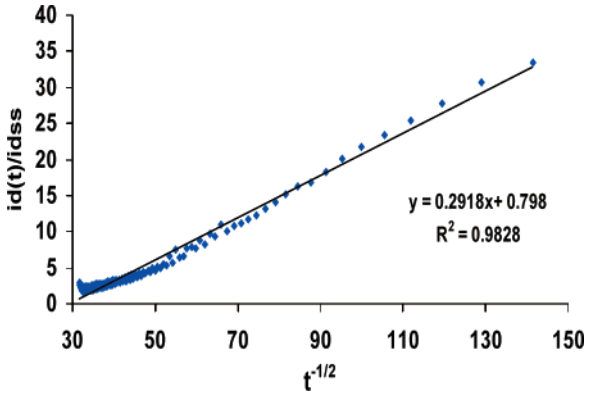

Figure 2. Plot of the experimental ratio $id(t)/idss$ against the inverse square root of time for the oxidation of 0.4 mM **T1** in MeCN/Bz (1:1 v/v), 0.1 M $TBAPF_6$, with a 10 μm diameter Pt microdisc; the sampling rate is 10 μs per point. The results of the linear regression are also shown.

sealed bottle) and anhydrous benzene (Bz, 99.9% in a sure-sealed bottle) were obtained from Aldrich. Tetra-*n*-butylammonium hexafluorophosphate ($TBAPF_6$) was recrystallized twice by adding it to heated ethyl acetate, followed by cyclohexane added dropwise, until a cloudy haziness was observed. The crystals were then dried in a vacuum oven at 100 °C prior to transferring directly into an inert-atmosphere dry box (Vacuum Atmospheres Corp, Hawthorne, CA). Tetra-*n*-butylammonium oxalate (TBAOX) was prepared by mixing oxalic acid (EM Science) and tetra-*n*-butylammonium hydroxide in methanol (Fluka) in a mole ratio of 1:2 followed by evaporation and drying in a rotary evaporator. All solutions were prepared in the dry box in an airtight cell for measurements completed outside the dry box.

Apparatus and Instrumentation. UV−vis spectra were recorded on a Milton Roy Spectronic 3000 array spectrophotometer. Fluorescence spectra were recorded on a Fluorolog-3 spectrofluorimeter (ISA-Jobin Yvon Horiba, Edison, NJ) using a 1 cm path length quartz cuvette. The ECL spectra were taken using a charge-coupled device (CCD) camera (Princeton Instruments, SPEC-10). ECL intensity−time curves were collected using an Autolab potentiostat (Ecochemie) also connected to a photomultiplier tube (PMT, Hammatsu, R4220p). The PMT was supplied with 750 V from a high-voltage power supply, series 225 (Bertan High Voltage Corp, Hucksville, NY). Cyclic voltammograms (CVs) were recorded on a Model 660 electrochemical workstation (CH Instruments, Austin, TX). The working electrode was an inlaid Pt disc (0.5 mm diameter) [or a Pt microelectrode (10 μm diameter) for short-time chronoamperometry]; a 2 mm diameter, J-shaped electrode was used for ECL intensity measurements. All electrodes were polished on a felt pad with 0.3 μm, followed by 0.05 μm, alumina (Buehler Ltd., Lake Bluff, IL), sonicated in water and then in absolute EtOH for 5 min, and finally dried in an oven at 100 °C before transferring to the dry box. A Pt wire served as a counter electrode and an Ag wire as a quasi-reference electrode (QRE). All potentials were calibrated against SCE by the addition of ferrocene as an internal standard after a series of measurements, taking $E^o_{Fc/Fc+} = 0.424$ V versus SCE.

All ECL measurements were performed as previously described.[28] To generate the ion annihilation reaction, the working electrode was pulsed between the first oxidation and reduction peak potentials with a pulse width of 0.1 s.

Digital simulations of the cyclic voltammograms were carried out with the DigiElch software package[29] to investigate the mechanisms of the electrochemical processes.

Results and Discussion

Electrochemistry of T1−T4. All electrochemical measurements were carried out in 1:1 v/v of MeCN/Bz (except for **T4** where, because of poor solubility, 1:2 v/v MeCN/Bz was used instead) with 0.1 M $TBAPF_6$ as the supporting electrolyte. Although cyclic voltammetry studies of **T1**−**T4** had been performed previously with oxidation in CH_2Cl_2 and reduction in THF,[23] these solvents are not appropriate for ECL because they have rather narrow potential windows. CVs of **T1** and **T2** in MeCN/Bz at a scan rate of $\nu = 0.5$ V/s showed two anodic reversible waves and a single reversible cathodic wave before background oxidation of the solvent/supporting electrolyte (Figure 1 and Supporting Information, Figures S1−S4), while **T3** showed two reversible anodic waves and two reversible cathodic waves. Oxidation of **T4** showed two reversible anodic waves followed by a split quasi-reversible second wave and then an irreversible peak that partially overlapped with the background, and two reversible cathodic waves followed by a smaller, less well-defined second wave. The observed peak

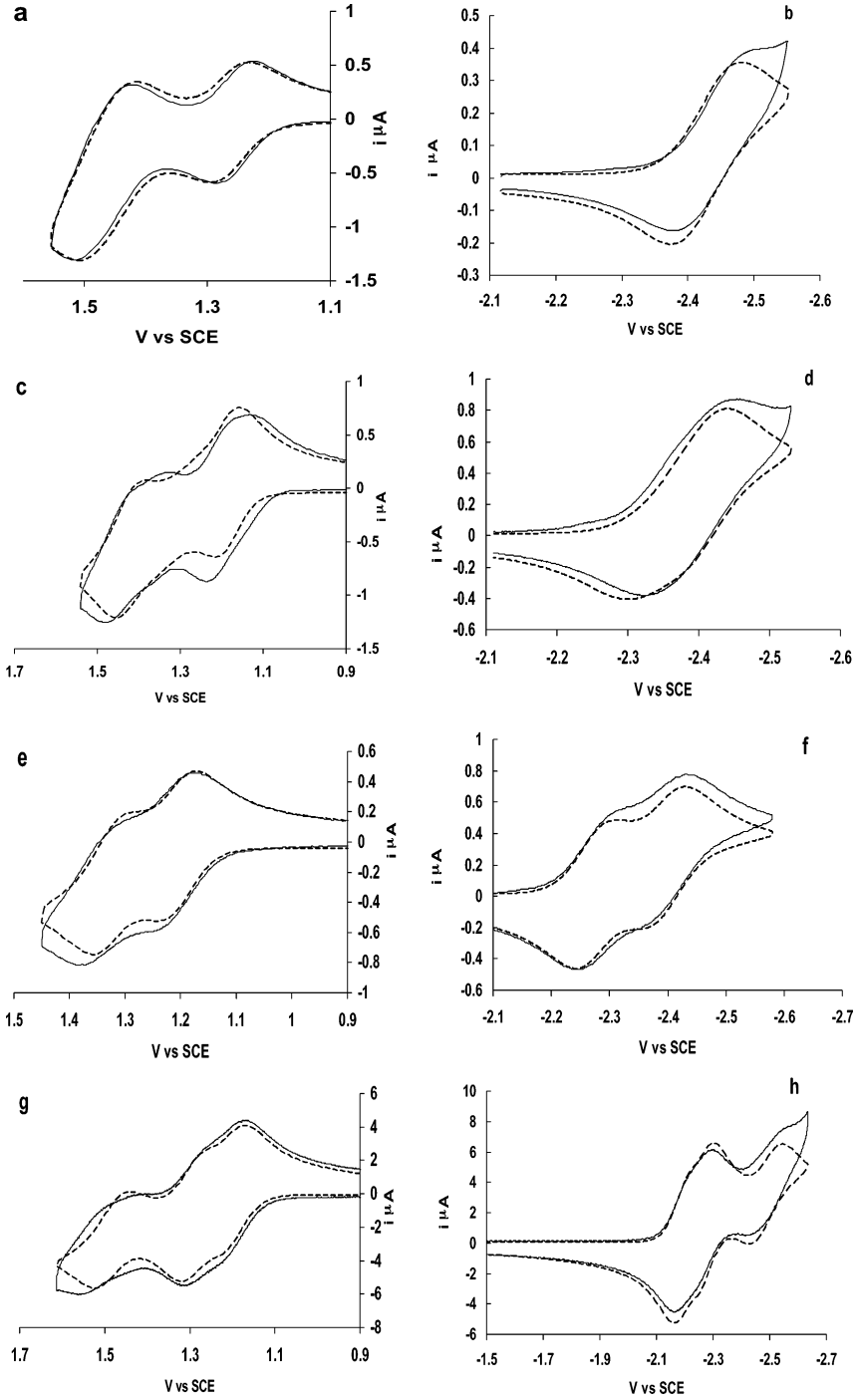

Figure 3. Comparison between simulated and experimental oxidation and reduction waves for **T1**−**T4** at 1 V/s. The model for these simulations: oxidation (a) **T1** (E,EE; $k^o_1 = 0.01$ cm/s, $k^o_2 = 0.1$ cm/s, $k^o_3 = 0.5$ cm/s), (c) **T2** (E,EE; $k^o_1 = 0.1$ cm/s, $k^o_2 = 0.01$ cm/s, $k^o_3 = 0.5$ cm/s), (e) **T3** (E,E; $k^o_1 = 0.06$ cm/s, $k^o_2 = 0.02$ cm/s), (g) **T4** (E,E,E; $k^o_1 = 1$ cm/s, $k^o_2 = 3$ cm/s, $k^o_3 = 0.1$ cm/s); reduction (b) **T1** (E; $k^o = 0.01$ cm/s at 0.5 V/s), (d) **T2** (E, $k^o = 0.01$ cm/s), (f) **T3** (E,E; $k^o_1 = 0.08$ cm/s, $k^o_2 = 0.05$ cm/s), (h) **T4** (E,E,E; $k^o_1 = 0.5$ cm/s, $k^o_2 = 0.5$ cm/s, $k^o_3 = 0.01$ cm/s); - - - simulated, — experimental.

splitting (ΔE_p) for the reversible waves was ∼100 mV, larger than the expected Nernstian one−electron wave ΔE_p of ∼59 mV. However, the internal standard, ferrocene, which is known to show Nernstian behavior, showed a similar ΔE_p under these same electrolyte conditions, suggesting that uncompensated resistance (∼2 kΩ), frequently observed with aprotic solvents, is the cause of the slightly larger ΔE_p values. All peak potentials of oxidations (E_{pa}^{ox}) and reductions (E_{pc}^{red}) are summarized in Table 1. Scan rate studies showed that the anodic and reverse cathodic peak currents of the first oxidation waves (i_{pa}^{ox}, i_{pc}^{ox}) were proportional to $v^{1/2}$. Additionally, the peak current ratio for the first oxidation waves of **T1**−**T4** (i_{pa}^{ox}/i_{pc}^{ox}) was approximately unity down to a scan rate of 50 mV/s, indicating the absence of significant contributions from following chemical reactions (Supporting Information, Figures S5−S13).

Diffusion coefficients, *D*, were found by plotting the peak current versus $v^{1/2}$ and are listed in Table 1, assuming each wave was a single electron-transfer step. To confirm the $n = 1$ assumption, chronoamperometric measurements for **T1** were also carried out at an ultramicroelectrode (UME) (Figure 2).[30] With this technique, *D* can be determined without knowledge of *n* or concentration (*C*), and *n* can be determined from the

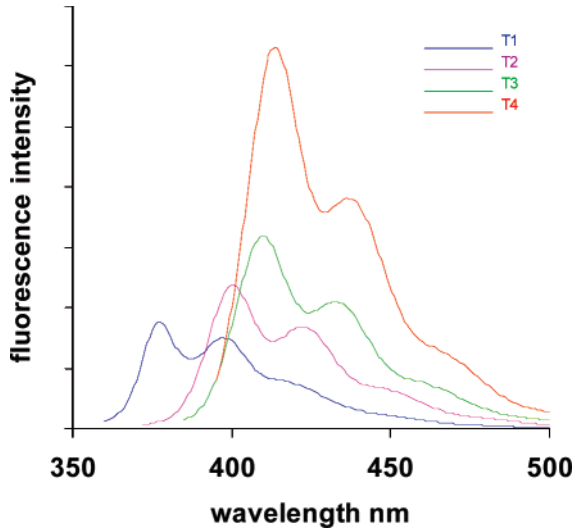

Figure 4. Fluorescence spectra of 0.02 μM **T1**−**T3** in a mixture of MeCN/Bz (1:1 v/v) and 0.02 μM **T4** in MeCN/Bz (1:2 v/v).

steady-state limiting current, if C is known. The D value found from the current transient agreed with that from CV, which confirmed the $n = 1$ nature of the reduction wave (this was also confirmed by comparison with CV i_p values for the oxidation process). For the oligomers **T1**−**T4**, there was a positive shift in E_{pc}^{red} (from −2.52 to −2.23 V vs SCE) and a negative shift in E_{pa}^{ox} for **T1**−**T4** (from +1.28 to +1.23 V vs SCE) with an increase of the size of molecules. This can be attributed to easier reduction and oxidation with increased delocalization. In summary, the results are consistent with formation of stable radical anions and radical cations for the first electron-transfer reactions, consistent with good ECL behavior.

Digital simulations of the CVs at different scan rates were carried out and compared to the experimental results to obtain better insight into the mechanisms and rates of both the anodic and cathodic reactions; the results are summarized in Table 1 (see also Figure 3 and Supporting Information, Figures S5−S13). The uncompensated resistance and capacitance were determined by performing a potential step in the relevant solvent system in a region where Faradaic reactions did not appear. The geometric electrode surface area used in simulations was determined by a potential step experiment performed in a solution of ferrocene in acetonitrile ($D = 1.2 \times 10^{-5}$ cm^2/s).

Although both the first anodic and first cathodic wave always involved a single electron transfer, the nature of the waves depended on the chain length. The cathodic CV of **T1** was characterized by one reversible electron transfer, with a heterogeneous rate constant, k^o, of about 0.01 cm/s (assuming complete resistance compensation) (Figures 3b and Supporting Information, Figure S7). The cathodic reaction for **T2** also showed one reversible electron transfer, with i_{pc}^{red} essentially the same as i_{pa}^{red} for the reoxidation (3×10^{-7} A) (Figure 3d and Supporting Information, Figure S9). In contrast, the cathodic scan of **T3** showed two reversible electron transfers with nearly the same peak current values for both reduction waves, indicating $n = 1$ for both reduction processes ($k^o_1 = 0.08$ cm/s, $k^o_2 = 0.05$ cm/s), which corresponds to the formation of radical anion and dianion species (Figure 3f and Supporting Information, Figure S11). The first and second reduction waves were essentially Nernstian, with i_{pa}^{red} and i_{pc}^{red} proportional to $\nu^{1/2}$, indicating diffusion control. **T4** showed two reduction waves, with the first composed of two reversible peaks that partially overlap at −2.23 V versus SCE for the first one and −2.31 V versus SCE for the second. The $i_{pc}^{red} \sim 9.25 \times 10^{-7}$ A for both overlapped peaks, which is approximately two times larger than the i_{pc}^{red} for **T1** and **T2**, suggesting the reduction peak is an overall two electron-transfer reaction, followed by another quasi-reversible peak at −2.57 V versus SCE (Figure 3h and Supporting Information, Figure S13).

TABLE 2: Summary of Spectroscopic Data

compound	absorbance, λ_{max} (nm) (log ϵ)	fluorescence, λ_{max} (nm)
T1	343 (5.07)	377, 398, 416sh
T2	362 (5.24)	400, 424, 452sh
T3	372 (5.41)	410, 434, 457sh
T4	377 (5.46)	414, 438, 467sh

The anodic CV of **T1** was characterized by two reversible waves. The first anodic peak was a one-electron transfer ($i_{pa}^{ox1} \sim 3 \times 10^{-7}$ A), while the second peak was about twice as high ($i_{pa}^{ox2} \sim 5 \times 10^{-7}$ A), suggesting $n = 2$ (Figure 3a and Supporting Information, Figures S5, S6). This mechanism was supported by simulation results, using a heterogeneous electron transfer for the first peak of $k^o = 0.01$ cm/s. The same trend was observed for the **T2** oxidation, with the first anodic wave of $n = 1$ and the second wave of $n = 2$, as two partially overlapped peaks, as demonstrated by simulation (Figure 3c and Supporting Information, Figure S8). However, the longer oligomer, **T3**, showed two consecutive reversible oxidations with nearly the same peak current values ($\sim 3 \times 10^{-7}$ A), indicating the same number of electrons ($n = 1$) were involved in both oxidation processes (Figure 3e and Supporting Information, Figure S10). This was confirmed by simulations of the difference in behavior with the shorter oligomer, **T1**, where the second oxidation wave was twice as large as the first, suggesting some difference in the electronic interactions between the oligofluorene arms and the truxene core or a difference in ion pairing of the two species. The longest oligomer, **T4**, showed a broadened wave of two partially overlapping peaks at +1.23 and +1.35 V versus SCE, followed by a reversible peak at +1.54 and an irreversible peak at +1.79 V versus SCE. Simulation indicated that the first wave consisted of two overlapping peaks (Figure 3g and Supporting Information, Figure S12).

These results can be interpreted as interplay of the charge delocalization over the arms and electronic interactions between the arms in **T1**−**T4**. For shorter oligomers, **T1** and **T2**, the truxene core is substantially involved in an initial one-electron transfer during the oxidation process. As a result, the next anodic electron transfer occurs at substantially higher potentials ($\Delta E_{pa}^{(ox1-ox2)} = 0.23$ and 0.24 V for **T1** and **T2**, respectively; Table 1). It involves the arms, as there is not good charge delocalization with the truxene cation radical. The next two electron transfers occur at about the same potential ($\Delta E = 0.05$ V, from simulation; Table 1), that is, essentially no interaction between the arms. The longer oligomer **T3** demonstrates better delocalization of the charge on the arm. Thus, the first oxidation has a smaller effect on the further electron-transfer potential resulting in decreased $\Delta E_{pa}^{(ox1-ox2)} = 0.16$ V; the arms interact in a stepwise one-electron process. In the longest oligomer **T4**, the radical cation is almost completely delocalized over the terfluorene arms, increasing the interactions between the arms; therefore, further decrease in splitting of the two first electron transfers is observed ($\Delta E_{pa}^{(ox1-ox2)} = 0.12$ V). Next (third), one-electron oxidation in **T4** is significantly shifted (by 0.19 V; cf. 0.05 V for **T1** and **T2** from simulation), indicating increased interaction between the arms (Table 1).

Spectroscopy. The truxene−fluorene oligomers are highly

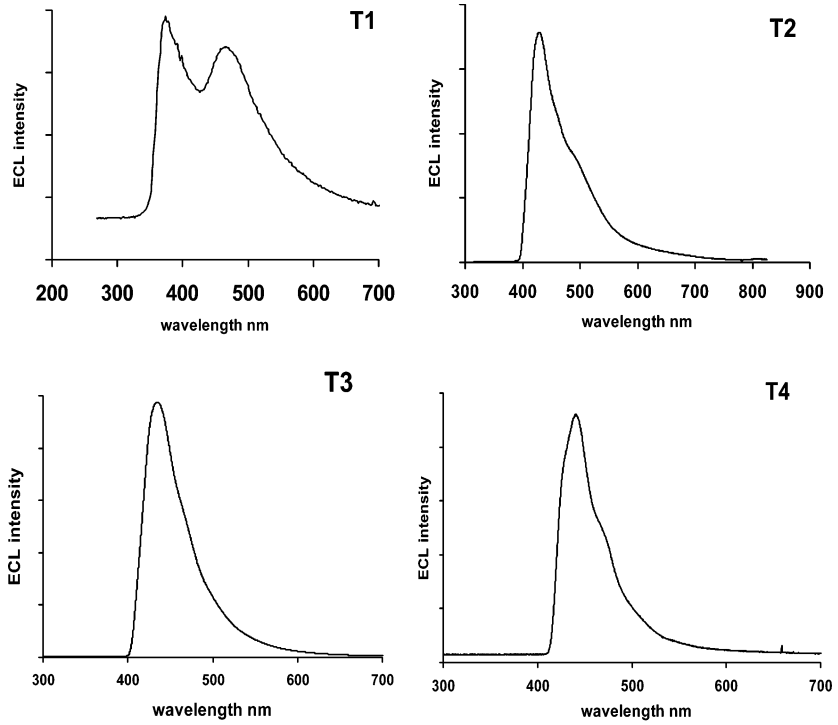

Figure 5. ECL spectra of 0.4 mM **T1**−**T3** in MeCN/Bz (1:1 v/v) and 0.4 mM **T4** in MeCN/Bz (1:2, v/v) with 0.1 s pulses by alternating the potential between +1.65 and −2.21 V versus Ag wire (QRE) for **T1**, +1.6 and −2.22 V for **T2**, +1.58 and −1.95 V for **T3**, and +1.5 and −2.3 V versus Ag wire for **T4**. The integration time was 3 min.

TABLE 3: ECL Peaks of Ion Annihilation Reactions and Fluorescence Emission

compound	ECL, λ_{max} (nm)	fluorescence, λ_{max} (nm)
T1	377, 470	377, 398
T2	425	400, 424
T3	434	410, 434
T4	443	414, 438

TABLE 4: Physical Data of the Ion Annihilation Reaction for ECL

compound	E_{pa}^{ox} (V vs SCE)[a]	E_{pc}^{red} (V vs SCE)[b]	$-\Delta G_{ann}$ (eV)[c]	$-\Delta H_{ann}$ (eV)[d]	E_s (eV)[e]
T1	+1.28	−2.52	3.80	3.70	3.29
T2	+1.24	−2.45	3.69	3.59	3.10
T3	+1.24	−2.30	3.54	3.44	3.02
T4	+1.23	−2.23	3.46	3.36	2.99

[a] Oxidation, anodic peak potentials of **T1**−**T3** in MeCN/Bz (1:1 v/v) and **T4** in MeCN/Bz (1:2 v/v); 0.1 M $TBAPF_6$. [b] Reduction, cathodic peak potentials of **T1**−**T4** V versus SCE. [c] $-\Delta G_{ann} = E_{pa}^{ox} - E_{pc}^{red}$. [d] $-\Delta H_{ann} = -\Delta G_{ann} - 0.1$.[32] [e] $E_s = 1239.85/\lambda_{max}^{PL}$ (nm).

fluorescent species both in solution and in the solid state, with the photoluminescence quantum efficiencies (ϕ_{PL}) for higher oligomers close to those for linear polyfluorene. Absorption and fluorescence spectra were taken in the same solvent systems as those used for electrochemistry (1:1 v/v MeCN/Bz for **T1**−**T3** and 1:2 v/v MeCN/Bz for **T4**) (Figure 4 and Supporting Information, Figure S14). The results are summarized in Table 2. The fluorescence spectra of **T1**−**T4** taken with an excitation at the absorption maxima display a fine vibronic progression typical for rigid-rod oligofluorene/polyfluorene structures. The position of the absorption and fluorescence peaks shifted toward the red from **T1**−**T4**, again consistent with increasing delocalization. The intensity of fluorescence was increased from **T1** to **T4**, and no luminescence above 500 nm was observed.

Electrogenerated Chemiluminescence (ECL): Ion Annihilation. When ECL was obtained by continuous pulsing (pulse width 0.1 s) between the first oxidation peak and the first reduction peak in the same solutions as those used in the electrochemical studies, with millimolar levels of **T1**−**T4**, all compounds produced ECL emission, with **T1** easily observed with the naked eye in a semidarkened room, and the longer oligomers **T2**−**T4** were seen even with the lights on. Typical ECL spectra are shown in Figure 5. Since the ECLs of **T2**−**T4** were very intense and could be seen with the naked eye, even under ambient lighting, a comparison of **T4** with 9,10-diphenylanthracene (DPA), a very bright ECL emitter, was carried out. The ECL from **T4** was about 80% of the ECL emission of DPA under the same conditions. However, the ECL of **T4** decreased to nondetectable levels after ∼1000 s of pulsing probably because of the formation of a polymer film on the surface of the electrode (anodic electropolymerization of oligofluorenes is described in the literature[31]). If the cell was returned to the glove box and the electrode polished after this loss of ECL, emission was again restored, consistent with filming of the electrode during pulsing.

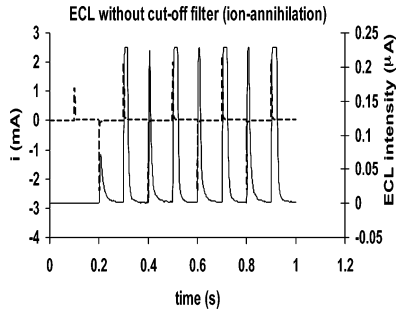

Figure 6. Intensity−time curve for annihilation ECL for compound **T1** with 0.1 s pulsing by alternating the potential between +1.65 and −2.21 V versus Ag wire QRE; - - - current, — light.

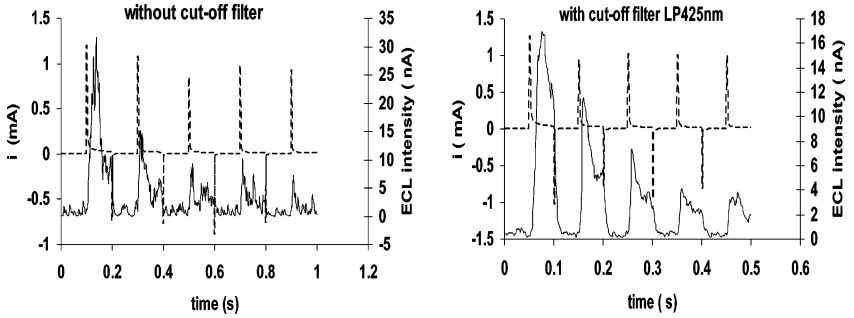

Figure 7. Intensity−time curve for coreactant ECL for compound **T1** with 0.1 s pulsing by alternating the potential between +1.65 and 0 V versus Ag wire QRE, without a cutoff filter and with a cutoff filter LP 425 nm; - - - current, — light.

The red shift observed in the ECL emission peaks proceeding from **T1**−**T4** is consistent with the fluorescence spectra (Table 3). The differences in the resolution due to the wider slit width (0.5−1 mm) used in recording the ECL spectra account for any apparent differences with the fluorescence spectra, except for **T1**. The energy available (enthalpy of annihilation, ΔH_{ann}) between the radical cations and radical anions of the oligomers for the annihilation reaction, as calculated from the electrochemical, E_p, results (shown in Table 4) is much greater than the singlet energy, E_s, from the emission spectra. Species **T2**−**T4** displayed ECL spectra that closely corresponded to the fluorescence emission. However, **T1** showed, in addition to the more intense emission corresponding to the fluorescence at 377 nm, a significant emission at a longer wavelength (470 nm) (Figure 5, Table 3). Such ECL is usually ascribed to emission from excimers or byproducts from side reactions of the radical ions. However, for **T1**, immediately after ECL measurement, the fluorescence spectrum of the solution was taken and found to be identical to that measured before ECL experiments, suggesting there were no side reactions to produce bulk byproducts fluorescing at longer wavelengths (consistent with the good stability of the radical ions).

The second possibility for the longer wavelength emission was the formation of an excimer that produces a structureless broad emission band. Such excimers (and the equivalent exciplexes) are sometimes found in ECL, even when they are not seen in photoluminescence, as a result of the direct formation by the ion annihilation reaction (eq 7).[33] Thus, we recently observed formation of excimers from poly(9,9-dioctylfluorene)[34] and ter(9,9-diaryl)fluorenes[20] in ECL experiments. If this is the case, the probability of a generated excimer would be much less if a coreactant was used as one of the reactants to generate ECL. To test this possibility, TBA oxalate was used as a coreactant. Oxalate ion generates a strong reductant, $CO_2^{-\bullet}$, following oxidation of oxalate,[17] as in eqs 9−11 below

$$C_2O_4^{2-} - e \rightarrow C_2O_4^{-\bullet} \quad (9)$$

$$C_2O_4^{-\bullet} \rightarrow CO_2 + CO_2^{-\bullet} \quad (10)$$

$$A^{+\bullet} + CO_2^{-\bullet} \rightarrow CO_2 + {}^1A^* \quad (11)$$

However, some excimers can also form from the route

$$A + CO_2^{-\bullet} \rightarrow CO_2 + A^{-\bullet} \quad (12)$$

followed by annihilation of the radical ions.

The emission from the ECL of the oxalate coreactant with **T1** was weak and could not be obtained with the CCD camera. However, we could study the ECL emission with the photomultiplier (PMT) using filters to estimate the emission wavelengths. To test the excimer, a LP-425 nm long-pass filter was used to cut off all wavelengths below 425 nm. As demonstrated in Figures 6 and 7, the ECL emission with the filter was close to the emission without it; therefore, excimer formation was not demonstrated.

Conclusions

Truxene−oligofluorene star-shaped oligomers show clean electrochemistry in a MeCN/Bz solution, with good stability of both the anion and cation radicals. They show intense blue EL emission that is clearly visible to the naked eye when generated by ion annihilation when the potential is pulsed between the first reduction and first oxidation potentials. The ECL emission for the larger oligomers, **T2**−**T4**, produce ECL spectra at the wavelengths very close to fluorescence emission, while **T1**, the smallest oligomer, also shows some longer wavelength emission of unknown origin.

Acknowledgment. We thank the National Science Foundation (CHE-0451494) for support of this research. K.M.O. was funded by a grant from the Ministry of Scientific Research and the University of Sulaimani, Kurdistan region, Iraq. A.L.K. was funded by EPSRC (GR/T28379).

Supporting Information Available: Additional CVs, ECL intensity−time curve, absorption spectra, and schemes. This material is available free of charge via the Internet at http://pubs.acs.org.

References and Notes

(1) Bard, A. J., Ed. *Electrogenerated Chemiluminescence*; Marcel Dekker: New York, 2004.

(2) (a) Perepichka, D. F.; Perepichka, I. F.; Meng, H.; Wudl, F. In *Organic Light-Emitting Materials and Devices*; Li, Z. R., Meng, H., Eds.; CRC Press: Boca Raton, FL, 2006; Chapter 2, pp 45−293. (b) Scherf, U.; List, E. J. W. *Adv. Mater.* **2002**, *7*, 477. (c) Neher, D. *Macromol. Rapid Commun.* **2001**, *22*, 1366. (d) Leclerc, M. *J. Polym. Sci., Part A: Polym. Chem.* **2001**, *39*, 2867. (e) Bernius, M. T.; Inbasekaran, M.; O'Brien, J.; Wu, W. *Adv. Mater.* **2000**, *12*, 1737.

(3) (a) Snaith, H. J.; Greenham, N. C.; Friend, R. H. *Adv. Mater.* **2004**, *16*, 1640. (b) Russell, D. M.; Arias, A. C.; Friend, R. H.; Silva, C.; Ego, C.; Grimsdale, A. C.; Müllen, K. *Appl. Phys. Lett.* **2002**, *80*, 2204.

(4) (a) Kim, Y.; Cook, S.; Choulis, S. A.; Nelson, J.; Durrant, J. R.; Bradley, D. D. C. *Chem. Mater.* **2004**, *16*, 4812. (b) Snaith, H. J.; Friend, R. H. *Thin Solid Films* **2004**, *451*−*452*, 567. (c) Zhang, F.; Perzon, E.; Wang, X.; Mammo, W.; Andersson, M. R.; Inganäs, O. *Adv. Funct. Mater.* **2005**, *15*, 745. (d) Kim, Y. M.; Lim, E.; Kang, I.-N.; Jung, B. J.; Lee, J.; Koo, B. W.; Do, L.-M.; Shim, H. K. *Macromolecules* **2006**, *39*, 4081.

(5) (a) Zaumseil, J.; Donley, C. L.; Kim, J.-S.; Friend, R. H.; Sirringhaus, H. *Adv. Mater.* **2006**, *18*, 2708. (b) Yan, H.; Yoon, M.-H.; Facchetti, A.; Marks, T. J. *Appl. Phys. Lett.* **2005**, *87*, 183501.

(6) (a) Rabe, T.; Hoping, M.; Schneider, D.; Becker, E.; Johannes, H.-H.; Kowalsky, W.; Weimann, T.; Wang, J.; Hinze, P.; Nehls, B. S.; Scherf, U.; Farrell, T.; Riedl, T. *Adv. Funct. Mater.* **2005**, *15*, 1188. (b) Heliotis,

G.; Xia, R.; Bradley, D. D. C.; Turnbull, G. A.; Samuel, I. D. W.; Andrew, P.; Barnes, W. L. *Appl. Phys. Lett.* **2003**, *83*, 2118. (c) Heliotis, G.; Bradley, D. D. C.; Turnbull, G. A.; Samuel, I. D. W. *Appl. Phys. Lett.* **2002**, *81*, 415.

(7) *Electronic Materials: The Oligomer Approach*; Müllen, K., Wegner, G., Eds.; Wiley-VCH: Weinheim, Germany, 1998.

(8) (a) Anémian, R.; Mulatier, J.-C.; Andraud, C.; Stéphan, O.; Vial, J.-C. *Chem. Commun.* **2002**, 1608. (b) Geng, Y.; Katsis, D.; Culligan, S. W.; Ou, J. J.; Chen, S. H.; Rothberg, L. J. *Chem. Mater.* **2002**, *14*, 463. (c) Katsis, D.; Geng, Y. H.; Ou, J. J.; Culligan, S. W.; Trajkovska, A.; Chen, S. H.; Rothberg, L. J. *Chem. Mater.* **2002**, *14*, 1332. (d) Geng, Y.; Trajkovska, A.; Katsis, D.; Ou, J. J.; Culligan, S. W.; Chen, S. H. *J. Am. Chem. Soc.* **2002**, *124*, 8337. (e) Geng, Y.; Culligan, S. W.; Trajkovska, A.; Wallace, J. U.; Chen, S. H. *Chem. Mater.* **2003**, *15*, 542. (f) Jo, J.; Chi, C.; Höger, S.; Wegner, G.; Yoon, D. Y. *Chem.—Eur. J.* **2004**, *10*, 2681. (g) Chi, C.; Im, C.; Enkelmann, V.; Ziegler, A.; Lieser, G.; Wegner, G. *Chem.—Eur. J.* **2005**, *11*, 6833. (h) Li, J.; Li, M.; Bo, Z. *Chem.—Eur. J.* **2005**, *11*, 6930. (i) Chi, C.; Wegner, G. *Macromol. Rapid Commun.* **2005**, *26*, 1532. (j) Li, Z. H.; Wong, M. S. *Org. Lett.* **2006**, *8*, 1499.

(9) (a) Geng, Y.; Trajkovska, A.; Culligan, S. W.; Ou, J. J.; Chen, H. M. P.; Katsis, D.; Chen, S. H. *J. Am. Chem. Soc.* **2003**, *125*, 14032. (b) Geng, Y.; Chen, A. C. A.; Ou, J. J.; Chen, S. H. *Chem. Mater.* **2003**, *15*, 4352. (c) Li, Z. H.; Wong, M. S.; Tao, Y.; Lu, J. *Chem.—Eur. J.* **2005**, *11*, 3285.

(10) (a) Wong, K.-T.; Chien, Y.-Y.; Chen, R.-T.; Wang, C.-F.; Lin, Y.-T.; Chiang, H.-H.; Hsieh, P.-Y.; Wu, C.-C.; Chou, C. H.; Su, Y. O.; Lee, G.-H.; Peng, S.-M. *J. Am. Chem. Soc.* **2002**, *124*, 11576. (b) Culligan, S. W.; Geng, Y.; Chen, S. H.; Klubek, K.; Vaeth, K. M.; Tang, C. W. *Adv. Mater.* **2003**, *15*, 1176. (c) Wong, K.-T.; Liao, Y.-L.; Lin, Y. T.; Su, H. C.; Wu, C. C. *Org. Lett.* **2005**, *7*, 5131. (d) Chen, A.-C. A.; Wallace, J. U.; Wei, S. K.-H.; Zeng, L.; Chen, S. H. *Chem. Mater.* **2006**, *18*, 204.

(11) Lupton, J. M.; Craig, M. R.; Meijer, E. W. *Appl. Phys. Lett.* **2002**, *80*, 4489.

(12) (a) List, E. J. W.; Guentner, R.; Scanducci de Freitas, P.; Scherf, U. *Adv. Mater.* **2002**, *14*, 374. (b) Gaal, M.; List, E. J. W.; Scherf, U. *Macromolecules* **2003**, *36*, 4236. (c) Gong, X.; Iyer, P. K.; Moses, D.; Bazan, G. C.; Heeger, A. J.; Xiao, S. S. *Adv. Funct. Mater.* **2003**, *13*, 325. (d) Romaner, L.; Pogantsch, A.; Scandiucci de Freitas, P.; Scherf, U.; Gaal, M.; Zojer, E.; List, E. J. W. *Adv. Funct. Mater.* **2003**, *13*, 597. (e) Gamerith, S.; Gadermaier, C.; Scherf, U.; List, E. J. W. *Phys. Status Solidi A* **2004**, *201*, 1132. (f) Sims, M.; Bradley, D. D. C.; Ariu, M.; Koeberg, M.; Asimakis, A.; Grell, M.; Lidzey, D. G. *Adv. Funct. Mater.* **2004**, *14*, 765.

(13) Faulkner, L. R. *J. Electrochem. Soc.* **1997**, *124*, 1724.

(14) Noffsinger, J. B.; Danielson, N. D. *Anal. Chem.* **1987**, *59*, 865.

(15) Zu, Y.; Bard, A. J. *Anal. Chem.* **2000**, *72*, 3223.

(16) Miao, W.; Choi, J.-P.; Bard, A. J. *J. Am. Chem. Soc.* **2002**, *124*, 14478.

(17) Chang, M.-M.; Saji, T.; Bard, A. J. *J. Am. Chem. Soc.* **1977**, *99*, 5399.

(18) Rubinstein, I.; Bard, A. J. *J. Am. Chem. Soc.* **1981**, *103*, 512.

(19) White, H. S.; Bard, A. J. *J. Am. Chem. Soc.* **1982**, *104*, 6891.

(20) Choi, J.-P.; Wong, K.-T.; Chen, Y.-M.; Yu, J.-K.; Chou, P.-T.; Bard, A. J. *J. Phys. Chem. B* **2003**, *107*, 14407.

(21) Wu, C.; Malinin, S. V.; Tretiak, S.; Chernyak, V. Y. *Nat. Phys.* **2006**, *2*, 631.

(22) (a) Zhou, X.-H.; Yan, J.-C.; Pei, J. *Org. Lett.* **2003**, *5*, 3543. (b) Li, B.; Li, J.; Fu, Y.; Bo, Z. *J. Am. Chem. Soc.* **2004**, *126*, 3430. (c) Li, B.; Xu, X.; Sun, M.; Fu, Y.; Yu, G.; Liu, Y.; Bo, Z. *Macromolecules* **2006**, *39*, 456. (d) Montes, V. A.; Pérez-Bolívar, C.; Agarwal, N.; Shinar, J.; Anzenbacher, P., Jr. *J. Am. Chem. Soc.* **2006**, *128*, 12436. (e) Lai, W.-Y.; Zhu, R.; Fan, Q.-L.; Hou, L.-T.; Cao, Y.; Huang, W. *Macromolecules* **2006**, *39*, 3707.

(23) Kanibolotsky, A. L.; Berridge, R.; Skabara, P. J.; Perepichka, I. F.; Bradley, D. D. C.; Koeberg, M. *J. Am. Chem. Soc.* **2004**, *126*, 13696.

(24) (a) Geng, Y.; Fechtenkötter, A.; Müllen, K. *J. Mater. Chem.* **2001**, *11*, 1634. (b) Ponomarenko, S. A.; Kirchmeyer, S.; Elschner, A.; Huisman, B.-H.; Karbach, A.; Drechsler, D. *Adv. Funct. Mater.* **2003**, *13*, 591. (c) Pei, J.; Wang, J.-L.; Cao, X.-Y.; Zhou, X.-H.; Zhang, W.-B. *J. Am. Chem. Soc.* **2003**, *125*, 9944. (d) Nicolas, Y.; Blanchard, P.; Levillain, E.; Allain, M.; Mercier, N.; Roncali, J. *Org. Lett.* **2004**, *6*, 273. (e) Sun, Y.; Xiao, K.; Liu, Y.; Wang, J.; Pei, J.; Zhu, D. *Adv. Funct. Mater.* **2005**, *15*, 818. (f) Cravino, A.; Roquet, S.; Alévêque, O.; Leriche, P.; Frère, P.; Roncali, J. *Chem. Mater.* **2006**, *18*, 2584. (g) Cremer, J.; Bäuerle, P. *J. Mater. Chem.* **2006**, *16*, 874.

(25) (a) Holst, H. C.; Oehlhof, A. *Eur. J. Org. Chem.* **2003**, 4173. (b) Fratiloiu, S.; Senthilkumar, K.; Grozema, F. C.; Christian-Pandya, H.; Niazimbetova, Z. I.; Bhandari, Y. J.; Galvin, M. E.; Siebbeles, L. D. A. *Chem. Mater.* **2006**, *18*, 2118. (c) Brunel, J.; Mongin, O.; Jutand, A.; Ledoux, I.; Zyss, J.; Blanchard-Desce, M. *Chem. Mater.* **2003**, *15*, 4139.

(26) (a) Rodríguez, J. G.; Esquivias, J.; Lafuente, A.; Díaz, C. *J. Org. Chem.* **2003**, *68*, 8120. (b) Yamaguchi, Y.; Ochi, T.; Miyamura, S.; Tanaka, T.; Kobayashi, S.; Wakamiya, T.; Matsubara, Y.; Yoshida, Z. I. *J. Am. Chem. Soc.* **2006**, *128*, 4504.

(27) (a) Wang, Y.; He, G. S.; Prasad, P. N.; Goodson, T., III. *J. Am. Chem. Soc.* **2005**, *127*, 10128. (b) Yan, Y.-X.; Tao, X.-T.; Sun, Y.-H.; Wang, C.-K.; Xu, G.-B.; Yang, J.-X.; Ren, Y.; Zhao, X.; Wu, Y.-Z.; Yua, X.-Q.; Jiang, M.-H. *J. Mater. Chem.* **2004**, *14*, 2995.

(28) McCord, P.; Bard, A. J. *J. Electroanal. Chem.* **1991**, *318*, 91.

(29) (a) Rudolf, M. *J. Electroanal. Chem.* **2003**, *543*, 23. (b) Ruldolf, M. *J. Electroanal. Chem.* **2004**, *571*, 289. (c) Rudolf, M. *J. Electroanal. Chem.* **2003**, *558*, 171. (d) Rudolf, M. *J. Comput. Chem.* **2005**, *26*, 619. (e) Rudolf, M. *J. Comput. Chem.* **2005**, *26*, 633. (f) Rudolf, M. *J. Comput. Chem.* **2005**, *26*, 1193.

(30) Denuault, G.; Mirkin, M. V.; Bard, A. J. *J. Electroanal. Chem.* **1991**, *308*, 27.

(31) Hapiot, P.; Lagrost, C.; Le Floch, F.; Raoult, E.; Rault-Berthelot, J. *Chem. Mater.* **2005**, *17*, 2003.

(32) Santa Cruz, T. D.; Akins, D. L.; Birke, R. L. *J. Am. Chem. Soc.* **1976**, *98*, 1677.

(33) Lai, R. Y.; Fleming, J. J.; Merner, B. L.; Vermeij, R. J.; Bodwell, G. J.; Bard, A. J. *J. Phys. Chem. A* **2004**, *108*, 376.

(34) Prieto, I.; Teetsov, J.; Fox, M. A.; Vanden Bout, D. A.; Bard, A. J. *J. Phys. Chem. A* **2001**, *105*, 520.